Influence of topography on the optical performances of a Fresnel linear asymmetrical concentrator array: The case of the eLLO solar power plant

Edouard Montanet, Sylvain Rodat, Quentin Falcoz, Fabien Roget

Influence of topography on the optical performances of a Fresnel linear asymmetrical concentrator array: the case of the eLLO solar power plant

Edouard MONTANET[a,], Sylvain RODAT[a], Quentin FALCOZ[a], Fabien ROGET[b],*

[a] PROMES-CNRS laboratory, Odeillo, France

[b] eLLO solar power plant, Llo, France

E-mail address: edouard.montanet@promes.cnrs.fr

**Corresponding author*

Abstract

Solar field orientation and inclination are variables that significantly influence the optical performance over the year of Linear Fresnel Collector (LFC). The usual field configuration is a flat north-south (NS) orientation, however, the future development of the LFC sector, for example for solar heat for industry, could more often impose the land choice and therefore the solar field configuration. To study the influence of such configuration on a solar field optical performance, a ray-tracing model was used to evaluate the LFC optical performance for each solar position and a consistent methodology was developed to evaluate the solar position in the module reference system. This method allows studying the optical performance of any LFC array configuration. The paper first looks separately at the influence of orientation and tilt imposed by the topography of the eLLO project, then focuses on the eLLO solar power plant case study. The results of eLLO's solar line simulation showed an increase of 1.6% in annual absorbed energy compared to NS implementation, which is the best orientation for the localization. In conclusion, the design and implementation of modular LFC array can be adapted to a wide range of terrains and can even take advantage of this constraint.

Keywords:

Concentrated solar power, Linear Fresnel collector, Orientation and Inclination, Topography, Optical study.

Nomenclature

Acronyms

CSP	Concentrated Solar Power
LFC	Linear Fresnel Collectors
PTC	Parabolic Trough Collectors
DSG	Direct Steam Generation
LCOE	Levelized Cost Of Energy
MCRT	Monte-Carlo Ray Tracing
DNI	Direct Normal Irradiance
NS	North-South
EW	East-West
IAM	Incidence Angle Modifier

Latin symbols

A_{col}	collection area [m²]
E_{abs}	total absorbed energy [J]
E_{sol}	total incident solar energy [J]
A_0	solar azimuth [°]
h_0	solar elevation [°]

Greek symbols

$\theta_{\perp}$	angle made by the incident beam with the topocentric vertical axis in the transversal plane [°]
$\theta_{\parallel}$	angle made by the incident beam with the topocentric vertical axis in the longitudinal plane [°]
θ_i	angle made by the incident beam with its image in the transversal plane [°]
$\eta_{opt,max}$	maximum optical yield [%]
$\phi_{abs,zenith}$	solar absorbed power by the absorber for a solar position at the zenith of the module [W]

1. Introduction

According to the International Energy Agency, after stabilizing in 2014, 2015, and 2016 due to improvements in energy efficiency, global emissions began to climb again in 2017. This rise is attributable in part to rising electricity usage and increased CO_2 emissions from coal and gas power plants [1]. In 2018, the main sectors of activity emitting greenhouse gases in the world are electricity and heat production [1]. Thus, decarbonizing the electricity sector by developing emission-free production systems is becoming a major challenge in climate protection strategies [2].

Concentrating Solar Power (CSP) technologies are one of the promising solutions to reduce gas emissions in the energy sector [3] and have important advantages when compared to other renewable energies in terms of grid stability due to thermal energy storage. The Parabolic Trough Collector (PTC) technology is the most technically and commercially proven technology and represents, in 2021, 76% of the CSP installed capacity [4], the rest of the projects being solar tower technologies project and more marginally LFC technology [3].

However, the dominance of PTC technology is expected to fade as solar tower and LFC projects increase, driven by a lower Levelized Cost of Energy (LCOE) for both technologies [5]. Compared to the PTC technology, LFC is based on a simplified architecture due to its lower wind load, has easier manufactured mirrors, a fixed receiver which avoids the need of rotating joints [6] and enables direct steam generation (DSG) [7]. Thus, LFC technology has the greatest cost reduction potential among all CSP technologies [6,8].

Many design elements, including the number and width of mirrors, the height, and technology of the receiver, the distance between mirrors, the localization has been the topic of LFCs optical design optimization studies [9–16]. These optical optimizations are performed using simple geometric approaches and Monte-Carlo ray tracing codes. Besides, these methods were also used to investigate the optical performance of LFCs for different field orientation and inclination [17–22]. It should be noted that unusual designs have been studied, such as the compact linear Fresnel collector and the point focus Fresnel collector modules [23,24].

Solar field orientation is a unique variable of linear solar concentrated technologies, which significantly influences the optical performance over the year. The main orientations studied are NS and EW orientation. It is commonly recognized that NS orientation fields achieve a more constant optical performance during summer days. However, they admit low optical performance during winter, which can be limiting to reach high temperatures. Furthermore, due mainly to end-line losses and cosine losses, EW orientation fields provide high flux intensities at solar noon every day of the year, but low values in the morning and evening [19,20].

According to Abbas et al. [18], EW implantation appears to be more attractive for latitudes beyond the tropics, but NS orientation fields attain higher efficiency when the solar field is closer to the equator. Other LFCs implementation studies have been carried out as the orientation proposed by Alrwashdeh [17] which admits an offset of 45° from the north-south axis and the tilted solar fields toward the South studied by Abbas et al. [18] for a NS and EW orientation fields. Moreover, Sharma et al. [21] use geometric approaches to study the influence of NS and EW implementation for different localization to evaluate the cost of energy and the LCOE.

Nevertheless, most LFCs plants in operation are almost NS oriented or slightly offset. Table 1 lists LFCs plants, their orientation, and their localization. Huaqiang TeraSolar 15MW Fresnel plant and eLLO solar power plant have a significant offset from NS axis. Indeed, specific configuration of such a plant can be based on the potential performance gain as Huaqiang TeraSolar project, which chose an EW orientation and tilted module toward the South. The eLLO Solar Power plant was built in a mountainous area where land terracing was impossible due to particular environmental interest and high earthwork costs. Therefore, eLLO's solar field orientation and inclination was imposed by local topography; the design was also adapted to the topography using an asymmetrical distribution of primary reflectors bending radius, which is the only commercial plant with such a design.

Table 1 : List of Fresnel linear solar power plants and their orientation, adapted from [25]

Project name	**Localization**	**Latitude [°]**	**Longitude [°]**	**Offset from the NS axis**	**Current status**
Kimberlina Solar Thermal Power Plant	United States	35.6	-119.2	-10°	Non-operational
Liddell Power Station CSP Project	Australia	-32.4	151.0	5°	Non-operational
Puerto Errado 1 (PE1) Thermosolar Power Plant	Spain	38.3	-1.6	0°	Operational
Puerto Errado 2 (PE2) Thermosolar Power Plant	Spain	38.3	-1.6	0°	Operational
Dhursar	India	26.8	72.0	0°	Operational
Rende-CSP plant	Italy	39.4	16.2	-10°	Operational
Huaqiang TeraSolar 15MW Fresnel	China	41.2	114.6	80°	Operational
Dadri ISCC Plant	India	28.6	77.6	0°	Operational
Lanzhou Dacheng Dunhuang 10MW Fresnel	China	40.1	94.4	0°	Operational
Lanzhou Dacheng Dunhuang 50MW Fresnel	China	40.1	94.4	0°	Operational
eLLO solar power plant	France	42.5	2.1	-50.9°	Operational

This paper aims to give an optical approach to evaluate separately the influence of both orientation and inclination of eLLO LFC arrays and to assess the particular case of eLLO solar power plant. Section 2 describes the optical behavior of eLLO's module using MCRT software. Section 3 describes the orientation and inclination impact on the optical performance of a LFC arrays for both solstices' days and on an annual basis by modelling four configurations (NS flat configuration, EW flat configuration and eLLO-like flat and tilted configurations). Finally, the specific case of eLLO solar power plant is considered in Section 4 to show the potential gain of the configuration and design determined by SUNCNIM company.

2. Optical characterization of eLLO's linear Fresnel concentrator

2.1. eLLO's linear Fresnel concentrator design

The eLLO solar power plant, operated by SUNCNIM, is located on the Cerdan plateau, a mountainous region in the South of France (2.1°W; 42.5°N) (Figure 1). The plant was inaugurated in September 2019. It comes with unique features from thermodynamic and optical perspectives such as the steam storage system capacity, the solar tracking system simplification and the solar module configuration related to the constraints of the topography.

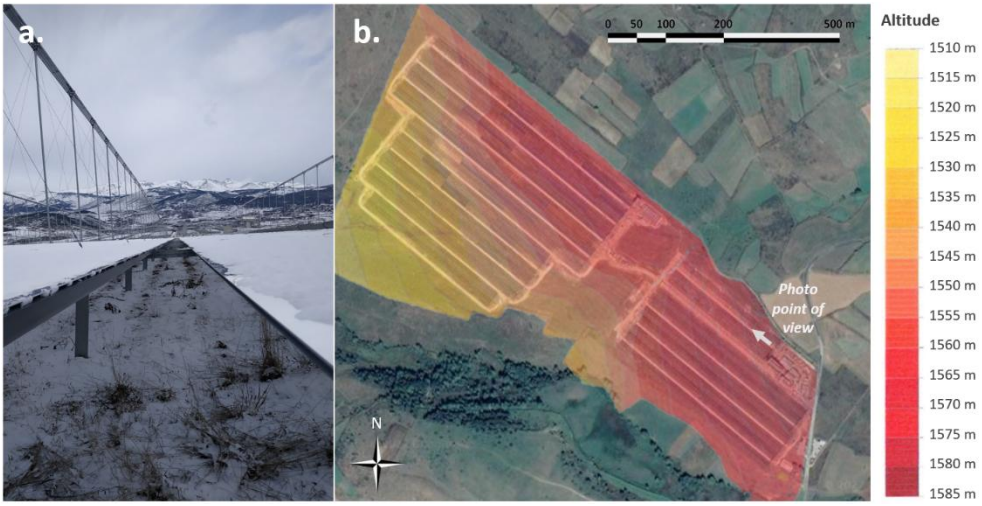

Figure 1: a. Photo of eLLO's solar lines ; b. topography of the site

This plant is based on a modular LFC technology, i.e. several modules in series form a solar line and several solar lines in parallel form a solar field. The solar modules developed by SUNCNIM are 67 m long and 18 m wide. Figure 2 shows a cross-section of an eLLO's module with the main components: the primary reflectors, the solar tracking system and the solar receiver which includes a secondary reflector and an absorber tube.

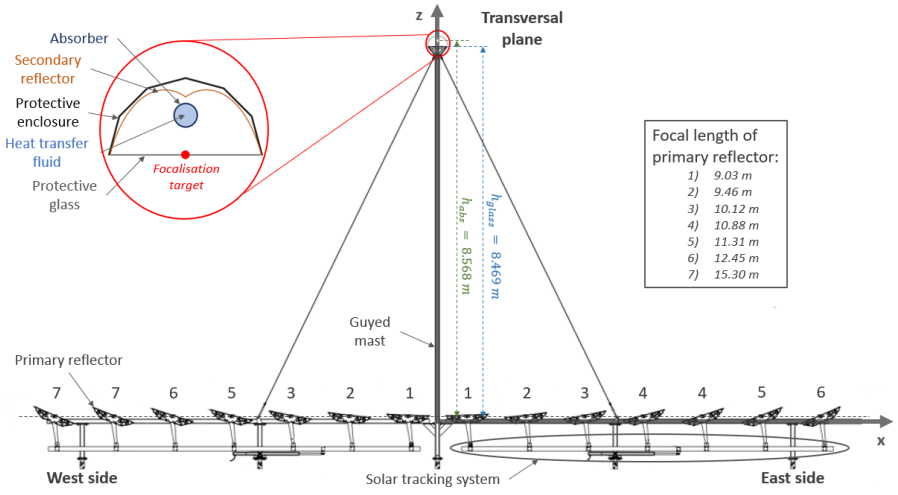

Figure 2 : Cross-section schematic representation of eLLO's linear Fresnel concentrator

The eLLO's module is equipped with 140 curved primary reflectors (902.2 m²) and a tracking system for both sides of the module that targets the aperture of the solar receiver. The number of primary reflectors in the longitudinal plane is identified as a number of spans to differentiate it from the number of rows in the transversal plane (Table 2).

The distribution of the primary reflectors bending radius is asymmetrical on each side of the vertical axis, and this specific distribution is presented in Figure 2. Generally, LFC modules are symmetrical. In the case of the eLLO solar power plant, the prototype developed by SUNCNIM at the beginning of the project was assembled with a symmetrical distribution of the primary reflectors bending radius [26]. However, the topographic constraints related to the impossibility of terracing because of the ecological interest area of the region, imposed the orientation and the inclination of the modules. This asymmetrical distribution of the bending radius of the primary reflectors is the result of an internal study (not detailed here) to optimize the optical performance without modification of design or manufacture of the eLLO module. However, in the case of eLLO solar power plant, the asymmetrical distribution is the result of an optimization study based on the optical behavior of oriented and tilted modules.

The solar receiver is installed at 8.5 m above the axes of the mirrors by several guyed masts and allows capturing the solar radiation coming from the primary concentrator. It is composed of an absorber tube, glass covers, protective enclosures and secondary reflectors shaped as Compound Parabolic Concentrator (CPC).

These elements are assembled in sections in the longitudinal direction, and the main characteristics and optical parameters of the primary concentrator and receiver are presented respectively in Table 2 and Table 3.

Table 2 : Geometric specification and optical properties of the primary concentrator components

Mirror optical properties	
Reflectivity	0.94
Slope error [mrad]	3
Specularity error [mrad]	1.5
Geometric specification of the primary concentrator	
Number of rows in the longitudinal plane (called span)	10
Shift between span [m]	Between 0.246 and 0.266
Number of rows in the transversal plane	14
Shift between row [m]	1.35
Number of primary reflectors [m]	140
Length of the primary reflectors [m]	6.444
Width of primary reflectors [m]	1
Focal length of primary reflectors [m]	Between 9 and 15

Table 3 : Geometric specification and optical properties of solar receiver components [27,28]

Optical properties of the protective glass	
Transmission (function of the incidence angle)	[0.952; 0]
Reflectivity (function of the incidence angle)	[0; 0.524]
Optical properties of the CPC secondary reflector	
Reflectivity	0.89
Slope error [mrad]	2
Specularity error [mrad]	1.5
Optical properties of the absorber tube	
Absorptivity of the absorber coating	0.945
Geometric specification of the solar receiver	
External radius of the absorber tube [cm]	4.445
Acceptance angle of CPC secondary reflector [°]	50.4°
Height between the glass and the primary reflectors axes [m]	8.469
Gap between the absorber tube and the secondary reflector [m]	0.01

The geometric concentration ratio, corresponding to the ratio between the primary reflectors width and the the absorber tube perimeter, is equal to 50 for the eLLO module. Thus, according to the ideal concentration expression, expressed by Rabl [29], the acceptance angle of the eLLO module is equal to 1.14°.

The optical properties of the glass cover are presented in the appendix, Figure A.1, and are dependent on the incidence angle between incident radiation and normal vector. It must be reminded that soiling issues must be considered as an important factor in optical performance analyses of concentration systems [30]. Nevertheless, in the present case, clean reflective surfaces only were considered.

Finally, the chosen orientation is a compromise between the number of modules to produce thermal energy needed and the available surface area. In summary, the eLLO's solar field is oriented with an offset of 50.9° from the NS axis and eLLO's modules are arranged to follow the topography of the site. The minimal, maximum, and average inclination of eLLO's module in the transverse and longitudinal planes are presented in Table 4. It should be noted that the transversal tilts are similar along eLLO's solar line, and the longitudinal tilts are individually defined for each module.

Table 4 : Minimal, maximal and average eLLO's module tilts in longitudinal and transversal plane

	Minimal	**Maximal**	**Average**
Longitudinal tilts	0,09°	4,73°	2,44°
Transversal tilts	3,42°	4,87°	4,05°

2.2. Optical performance of eLLO's module

2.2.1. MCRT code

MCRT codes are based on the observation of photons interactions on a given surface from a ray beam randomly generated from another [31]. The Tonatiuh program is one of the programs based on this MCRT method and stands out from other tools by its intuitive interface and the advantage of being able to automate the modelling of tens or even hundreds of reflectors. This code has been experimentally validated with data from different solar concentration facilities (Mini-Pegase in Odeillo [32]; solar system of the Plataforma Solar de Almería [33]) and, in our case, it will be used to run several ray-tracing simulations of an eLLO's module to estimate its optical performance for each solar position. Nevertheless, before any simulation, it is important to define solar parameters as the sunshape, the direct normal irradiation – DNI and the number of photons to simulate.

The sun has a finite size described by an angular radius of 4.65 mrad. In other words, the solar radiation that reaches the module can admit a certain angle with the normal vectors of the surfaces depending on the point of the solar disk from which it is emitted and causes different angles of reflection. Moreover, the luminance also depends on the point of the solar disk from which it is emitted. These phenomena can be expressed in Tonatiuh as a Pillbox sunshape or a Buie sunshape [34]. The Pillbox sunshape assumes a uniform radiation profile inside the solar disk, neglecting the gradient of circumsolar radiation. On the contrary, the Buie profile accepts a probabilistic distribution over the entire solar and circumsolar disk, regardless of geographical location. Schubnell [35] found that the Pillbox sunshape simulation resulted in a 5% overestimation of the conversion efficiency of solar furnaces and solar towers. This error remains within the expected accuracy, and the choice of the Pillbox sunshape is sufficient for comparative studies.

Lastly, the DNI was fixed at 1000 W/m² and the number of photons was set at 2,000,000 according to a sensitivity analysis.

2.2.2. Incidence Angle Modifier of eLLO's module

2.2.2.1. Indicators presentation

Figure 3 shows how to define the solar position in an LFC reference system in the longitudinal and transversal plane with $\theta_{\parallel}$ and $\theta_{\perp}$, the longitudinal and transversal angles and the longitudinal incidence angle θ_i.

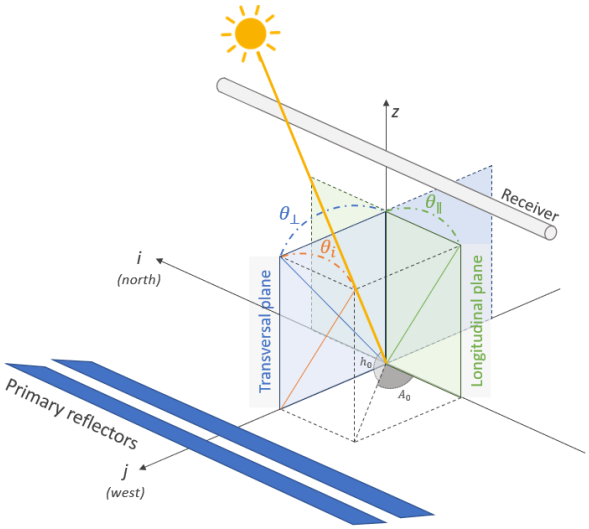

Figure 3 : Solar position in the transversal and longitudinal plane of a Linear Fresnel concentrator

Generally, the maximum optical efficiency is calculated as the solar absorbed power by the absorber divided by the incident solar power on the collection area for a solar position at the zenith of the module ($\theta_\parallel = 0°$ and $\theta_\perp = 0°$):

$$\eta_{opt,max} = \frac{\phi_{abs,zenith}}{DNI.A_{col}}, \quad (1)$$

where $\phi_{abs,zenith}$ is the absorbed solar power by the absorber tube when the sun is at the zenith of the module, DNI is the direct normal irradiance and A_{col} is the collection area defined as the sum of primary reflector area.

Then, the optical performance of LFC facilities decreases as the sun gets closer to the horizon. This intensification of optical losses, is considered in the definition of optical efficiency by the Incidence Angle Modifiers (IAM) defined in equation (2).

$$IAM(\theta_\parallel, \theta_\perp) = \frac{\eta_{opt}(\theta_\parallel, \theta_\perp)}{\eta_{opt,max}} \quad (2)$$

The IAMs can be determined during experimental campaigns or by modelling the concentrating system in a ray tracing software. The optical losses dependent on the solar radiation incidence angle are: the cosine losses, the losses by shading and blocking of primary reflectors and the end-line losses, since the receiver is not infinitely long and a part of the concentrated rays escapes further away.

These IAMs can be expressed as an optical efficiency matrix for each solar position [36] or as recommended by Mertins et al. [37–39], the IAM obtained by factoring the longitudinal IAM ($IAM_\parallel$) and transversal IAM ($IAM_\perp$) is a good approximation for LFC optical characterization. The $IAM_\parallel$ is calculated by simulating the optical behavior of the module when the transversal angle $\theta_\perp$ is null, and the $IAM_\perp$ is calculated by simulating the optical behavior of the module when the longitudinal angle $\theta_\parallel$ is null. The total IAM is then obtained by:

$$IAM(\theta_\parallel, \theta_\perp) = IAM_\parallel(\theta_\parallel) * IAM_\perp(\theta_\perp), \quad (3)$$

where $\theta_\parallel$ and $\theta_\perp$ are the longitudinal and transversal angles describing the solar position in the module reference system (see figure 3). These angles are a function of the solar position, defined by solar

azimuth A_0 and the elevation angle h_0. The solar azimuth value of 0° corresponds to the North and 90° corresponds to the East. Lastly, a solar elevation of 90° indicates that the sun is at the zenith.

The $IAMs$ presented in the literature are expressed with longitudinal angle ($\theta_{\parallel}$) and transversal angle ($\theta_{\perp}$) between [0°; 90°] for symmetric solar modules. However, since the study focuses on an asymmetric module (Figure 2), $IAMs$ will be evaluated for angles $\theta_{\perp}$ between $[-90°; 90°]$ and, for angle $\theta_{\parallel}$ between [0°; 90°]. With, $\theta_{\perp} = +90°$ corresponding to a solar position at the west of the module and $\theta_{\parallel} = +90°$ corresponding to a solar position at the north of the module.

2.2.2.2. Results

The ray tracing simulation goes all the way to the primary reflector, the absorber tube, considering the glass protection, the secondary reflector and finally the absorber tube. The longitudinal and transversal IAMs are obtained by analyzing the results of several ray tracing simulations of a module equipped with a quasi-infinite receiver of 335 m to eliminate the influence of end-of-line losses.

The simulation results are presented in Figure 4 and compared to IAMs of Nova-1 [40], LF-11 [41] and Heliotérmica [22], respectively the LFC module developed by the manufacturers Frenell - formerly Novatec, Industrial Solar and the LEPTEN laboratory, Brazil.

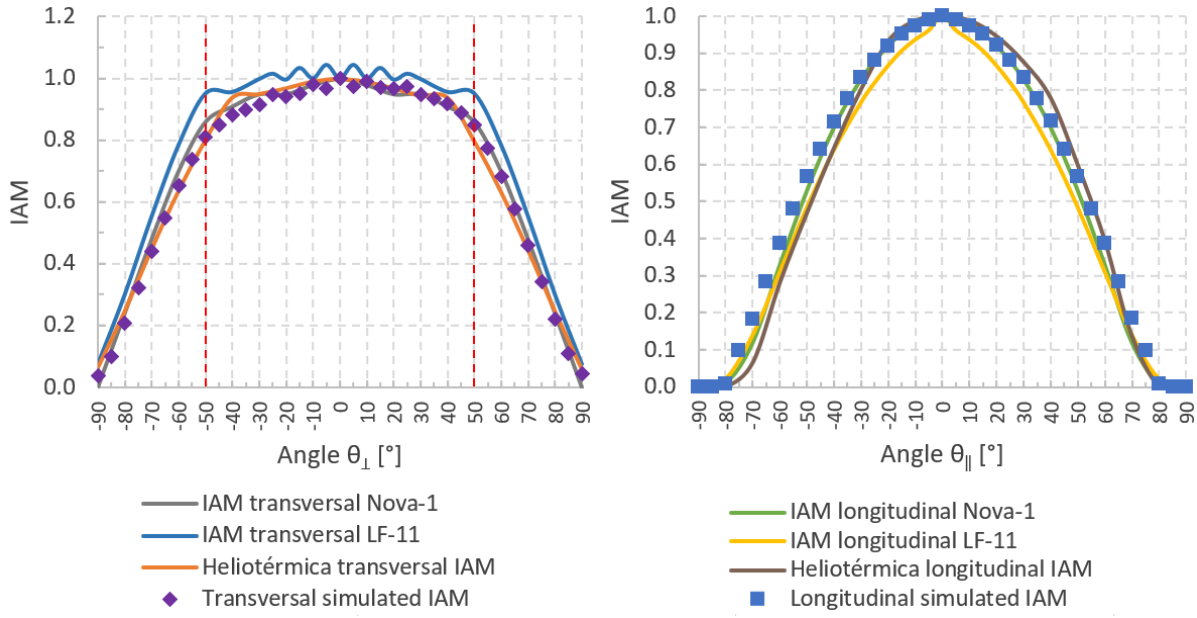

Figure 4 : eLLO's simulated IAMs compare to Nova-1, LF-11 and Heliotérmica IAMs

In general, it can be noticed that the global tendency of the 4 manufacturers are similar. The break in slope of the $IAMs_{\perp}$ is common to all 4 modules and can be explained by the sudden increase in optical losses due to blocking and shading phenomena. This break occurs for $\theta_{\perp} > 50°$ and $\theta_{\perp} < -50°$ for the Nova-1, LF-11 and eLLO module and for $\theta_{\perp} > 40°$ and $\theta_{\perp} < -40°$ for the Heliotérmica module.

Due to the asymmetrical modules, the simulated $IAM_{\perp}$ (purple diamonds) follows the trend of the Nova-1 $IAM_{\perp}$ (gray line) for $0° < \theta_{\perp} < 90°$, while for $-90° < \theta_{\perp} < 0°$ the simulated $IAM_{\perp}$ is slightly below the Nova-1 $IAM_{\perp}$.

Finally, the simulated $IAM_{\parallel}$ (blue squares) is the same for solar position on the north or south side of the module and is closer to the Nova-1 $IAM_{\parallel}$. Note that the simulated $IAM_{\parallel}$ is defined without end-line losses.

The results of our simulations are consistent with the results of the literature and describe well the expected behavior. Nevertheless, to be able to simulate a solar line, an $IAM_{\parallel}$ including end-line losses is calculated.

Table 5 shows the main specification of Nova-1, LF-11 and eLLO's modules, in terms of architecture.

Table 5 : Geometric specification and optical properties of the Nova-1, LF-11, Heliotérmica and eLLO's modules

Solar module name	**Nova-1**	**LF-11**	**eLLO**	**Heliotérmica**
Module width [m]	16.6	4.1	18	5
Module length [m]	44.8	7.5	67	12
Collection area [m²]	513.6	22	902.6	54
Number of rows in the longitudinal plane	8	3	10	12
Number of rows in the transversal plane	16	11	14	10
Number of primary reflectors	128	33	140	120
Height between the absorber tube and the axes of the primary reflectors [m]	7.4	4.5	8.6	3.75

The numbers of rows in the longitudinal and transversal plane of the Nova-1 module is closer to the number of rows of eLLO's module. Since the design of the Nova-1 module is close to the architecture of the eLLO's module, the optical behaviors of these two designs are similar.

The LF-11 module has an odd number of rows in transversal, i.e. the primary reflectors closest to the receiver are located directly below the receiver. That is why the maximum optical efficiency of the LF-11 module is reached for an angle $\theta_{\perp} = 5°$. Thus, LF-11 $IAM_{\perp}$ admit values greater than 1 because they are defined according to the optical efficiency at the zenith of the module. The variations of the LF-11 $IAM_{\perp}$ from $\theta_{\perp} = -20°$ to $20°$ could be explained by the shadow of the receiver on the primary concentrators; at $\theta_{\perp} = 0°$, the receiver shades the concentrators at the aplomb and at $\theta_{\perp} = 5°$, the shadow of the receiver blocks less solar concentration. Finally, the moving receiver proposed by Heliotérmica project can be observed in Figure 4b. It limits the end-line losses, here on one side of their module ($0° < \theta_{\parallel} < 90°$).

The asymmetrical distribution of primary reflectors bending radius is the result of an optimization study based on a preliminary optical convolution model. It indicated that a symmetrical distribution of primary reflectors bending radius around the receiver was not optimal for the configuration of eLLO's modules due to the specific module configuration, described in paragraph 2.1. As observed in Figure 4a, the optical performance of eLLO's module will be more important when the sun faces the west side than when it faces the east side of eLLO's modules. The annual optical behavior of symmetrical and asymmetrical modules will be discussed in paragraph 3.3 to highlight the impact of the asymmetrical eLLO's module design.

The results of our simulations are consistent with the results of the literature and describe well the expected behavior. Nevertheless, to be able to simulate a solar line, an $IAM_{\parallel}$ including end-line losses is calculated.

2.2.3. Incidence Angle Modifier with end-line losses

The end-line losses are due to the fact that the receiver is not infinitely long and that part of the photons escape further away. Figure 5 shows this loss effect occurring for non-zero angles $\theta_{\parallel}$ at the farthest line edge from the sun.

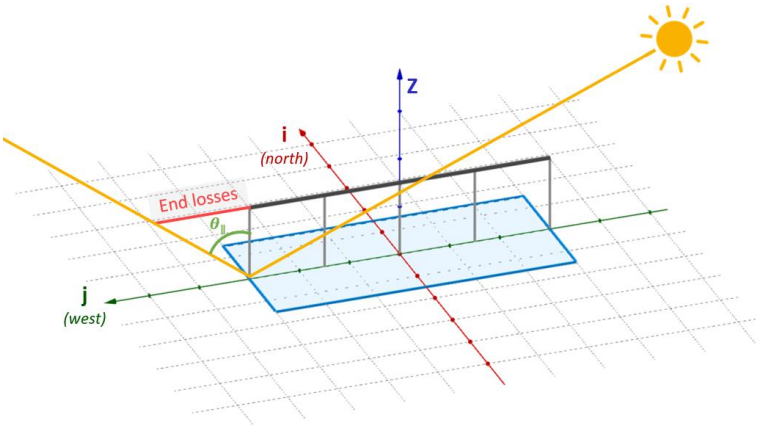

Figure 5 : End-line losses for an EW oriented Linear Fresnel concentrator

The simulated $IAM_{\parallel}$ was expressed with end-line losses by modelling a module equipped with a receiver of the length of the solar module, in contrast with the $IAM_{\parallel}$ without end-line losses defined in paragraph 2.2.2.2. Figure 6 shows the simulated $IAM_{\parallel}$ with and without end-line losses, noted respectively $IAM'_{\parallel}$ and $IAM_{\parallel}$. The equivalent loss length is calculated to estimate the shift of the focal line which occurs when $\theta_{\parallel}$ is not zero. This length corresponds to the ratio between end-line losses (W) and the linear absorbed power of the module equipped with a near-infinite receiver (W/m) and it is presented in Figure 5.

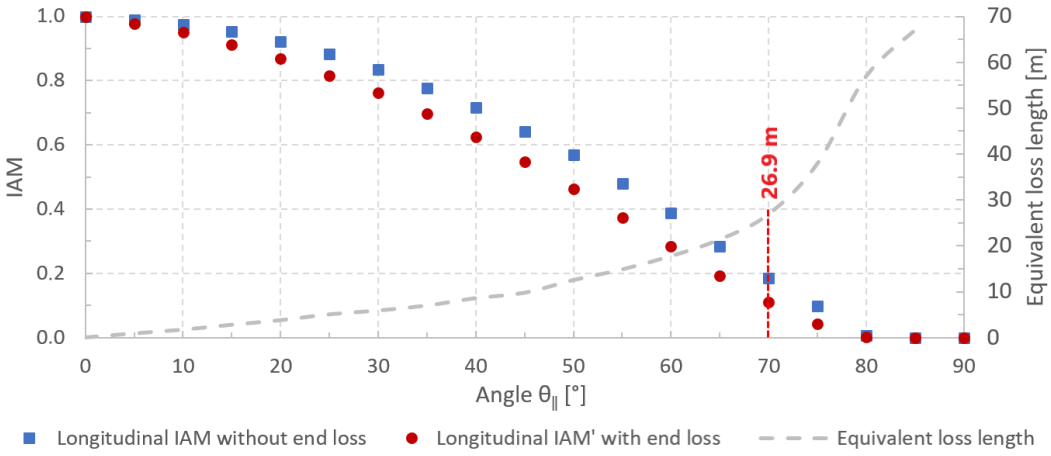

Figure 6 : Simulated longitudinal IAMs with and without end-line losses

The $IAM_{\parallel}$ is greater than $IAM'_{\parallel}$. The equivalent loss length is null for a sun position at the zenith of the module, and it increases with $\theta_{\parallel}$. Beyond $\theta_{\parallel} = 80°$, the optical efficiency of eLLO's module is zero, i.e. the optical losses tend towards infinity and end-line losses too. Thus, the equivalent loss length is superior to the 67 m long eLLO's module for $\theta_{\parallel} > 85°$, i.e. for longitudinal angles corresponding to zero optical performance.

For a NS flat configuration module, a solar position at $\theta_{\parallel} = 70°$ and $\theta = 0°$ and DNI equal to 1000 W/m², the total absorbed power without end-line losses per collection area of primary reflector is 130 W/m² and with end-line losses is 78 W/m², i.e. a loss of 52 W/m² corresponding to an equivalent loss length of 26.9 m. Considering a NS flat 6-modules line and the same solar position, the end-line losses correspond to 5.2% of the incident solar power impacting the primary concentrators.

Thus, the simulated $IAM_{\parallel}$ and $IAM'_{\parallel}$ make it possible to evaluate the optical performance of a solar line by considering end-line losses for the modules at the ends.

2.2.4. Mathematical model to compute the solar position in module reference system

To identify the IAMs for any LFC module configuration, a mathematical model is described to determine the position of the sun in the reference of the considered module configuration.

The solar position is computed using Grena's solar position algorithm #3 [42]. The results are expressed in spherical coordinates and are converted to Cartesian coordinates to calculate the solar position in the module reference system, according to equation (4):

$$\begin{pmatrix} x_0 \\ y_0 \\ z_0 \end{pmatrix} = \begin{pmatrix} \sin A_0 \cos h_0 \\ \cos A_0 \cos h_0 \\ \sin h_0 \end{pmatrix} \quad (4)$$

where, A_0 is the solar azimuth and h_0 is the solar elevation (Figure 3) and x_0, y_0 and z_0 are the Cartesian coordinates of the sun in topocentric coordinate system.

Thus, the coordinates of the sun in the module reference system are determined by the product of a transition matrix P^{-1} and the Cartesian coordinates of the sun in the topocentric reference system:

$$\begin{pmatrix} x_1 \\ y_1 \\ z_1 \end{pmatrix} = P^{-1} * \begin{pmatrix} x_0 \\ y_0 \\ z_0 \end{pmatrix} \quad (5)$$

In our case, different rotation matrices were used to determine the solar position in the reference system of each configuration studied. The new Cartesian coordinates (x_1, y_1, z_1) are then converted back to spherical coordinates to determine the $\theta_\perp$ and $\theta_\parallel$ angles.

$$h_1 = \sin^{-1} z_1 \quad (6)$$

For azimuths, the cases where the component following j_1 (horizontal axis pointing west) is positive and the case where the component i_1 (horizontal axis pointing south) is positive need to be distinguished.

$$A_1 = \sin^{-1}\left(\frac{x_1}{\cos h_1}\right), \qquad if\ j_1 > 0 \quad (7)$$

$$A_1 = \sin^{-1}\left(\frac{y_1}{\cos h_1}\right), \qquad if\ i_1 > 0 \quad (8)$$

Finally, the angle $\theta_\perp$ and $\theta_\parallel$ are defined by equation (9) and (10):

$$\theta_\perp = \tan^{-1}\left(\frac{x_1}{z_1}\right) = \tan^{-1}\left(\frac{\sin A_1}{\tan h_1}\right) \quad (9)$$

$$\theta_\parallel = \tan^{-1}\left(\frac{y_1}{\sqrt{x_1^2 + z_1^2}}\right) = \tan^{-1}\left(\frac{\cos A_1 \cos h_1}{\sqrt{(\cos A_1 \sin h_1)^2 + \sin^2 h_1}}\right) \quad (10)$$

Thus, for the location under study, the solar position is calculated with a 15 minute resolution for the studied days and DNI is provided by a clear sky model from the work of Bird et al. [43] available on the NREL website [4]. Finally, an optical efficiency value (η_{opt}) is assigned to all modules of the solar line at each instant from the IAMs (equation (2)).

Eventually, the daily optical yield ($\eta_{opt_{daily}}$) is calculated as the ratio between the total absorbed energy (E_{abs}) by the receiver and the total incident solar energy (E_{sol}) during a day.

$$E_{abs} = \int^{day} \alpha_{abs}.\left(\eta_{opt,max}.IAM_{\parallel}(\theta_i).IAM_{\perp}(\theta_{\perp})\right).DNI_{CS}.A_{col}.dt, \quad (11)$$

$$E_{sol} = \int^{day} DNI_{CS}.A_{col}.dt, \quad (12)$$

$$\eta_{opt_{daily}} = \frac{E_{abs}}{E_{sol}}, \quad (13)$$

where, α_{abs} is the absorptivity of the absorber, η_{opt_i} is the optical efficiency and DNI_{CS_i} is the clear-sky DNI.

3. Influence of Fresnel linear concentrators arrays topography on their optical performances

The purpose of this section is to offer a structured examination of how solar line configuration affects its optical performance, including the study of the orientations and inclinations influence. The 402 m long solar line studied is composed of 6 eLLO modules to be representative of the system installed in eLLO power plant. The optical performance of each configuration will be determined by identifying the IAMs corresponding to the solar position in the module coordinate system using a rotation matrix.

Note that for angle $\theta_{\perp} \neq 0°$, the solar position in the longitudinal plane is described using the longitudinal incidence angle θ_i shown in Figure 3 (θ_i replaces $\theta_{\parallel}$ in equation 3 [37,38]). Finally, optical performance is assessed along the year for eLLO's solar line configuration and both conventional NS and EW flat configurations for the localization of the eLLO plant.

3.1. Orientation impact on optical performance

First, the tree orientations described in Figure 7 are compared for the summer and winter solstice days. Each of these lines are flat, the orientation is either NS, EW or with an offset of 50.9° (eLLO's solar field orientation).

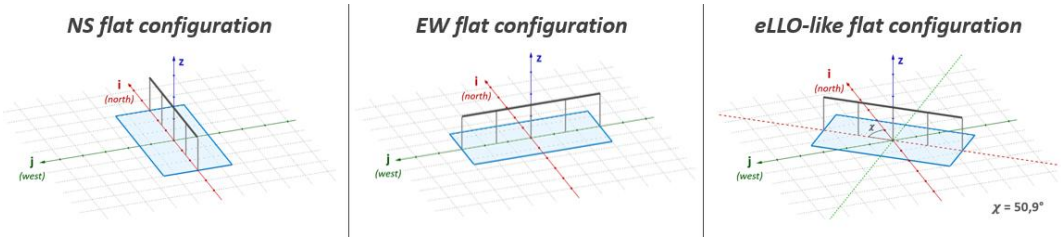

Figure 7: Three solar lines configurations with different orientations

The absorbed solar power evolution during a day for both solstices are shown, in Figure 8, for the three orientation cases.

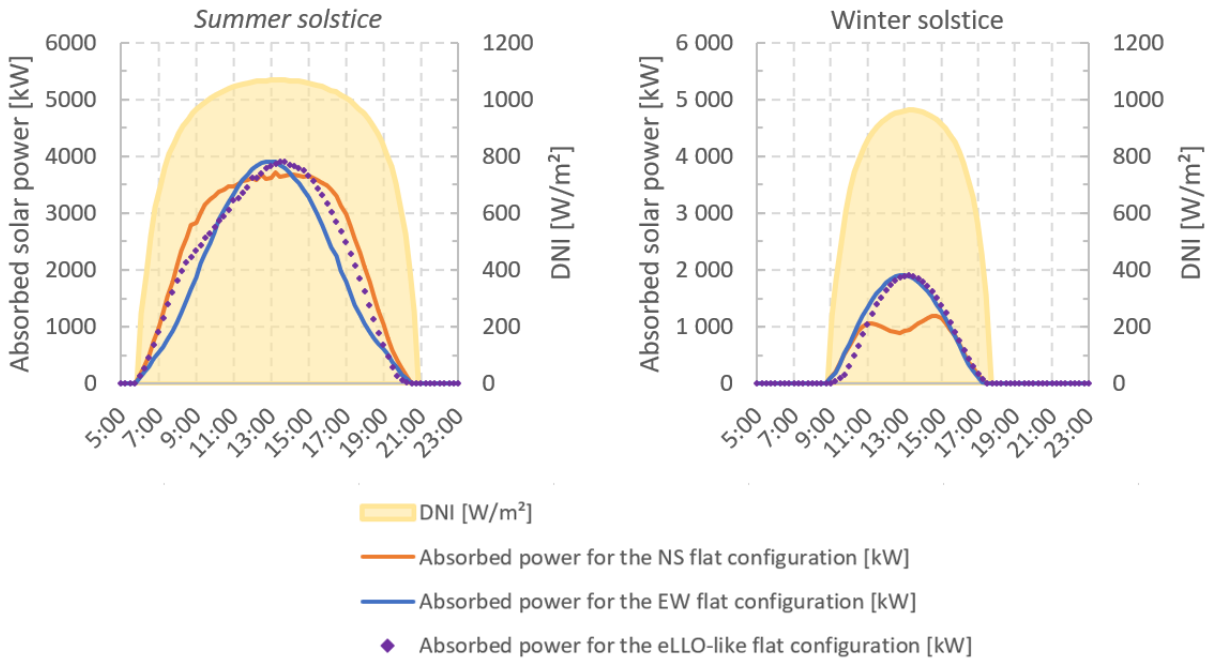

Figure 8 : Absorbed solar power by the NS and EW flat configuration and eLLO-like flat solar line for both solstices

NS and EW flat configurations results follow the same trends as the behavior described by Sebastian and al. [20] for a LFC plant. The total absorbed energy for NS implementation reaches a plateau for summer solstice day from 8 AM to 4 PM and two maximum values for winter solstice. For EW implementation, the total absorbed energy displays a bell shape curve for both solstice days.

The integrated daily results of the orientation impact study are summarized in Figure 9 and Table 6.

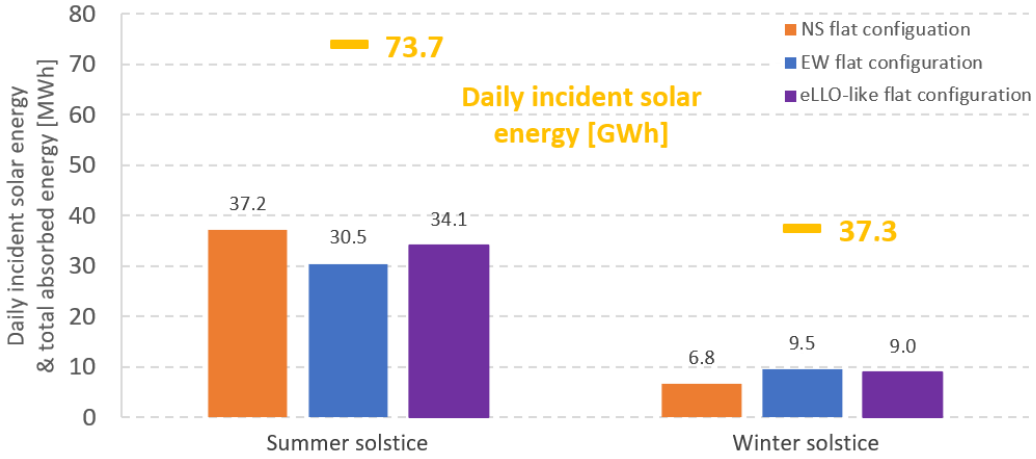

Figure 9 : Total absorbed energy for NS, EW and eLLO-like flat configuration for both solstices' days

Table 6 : Daily optical performance for NS, EW and eLLO-like flat configuration for both solstices' days

Day	NS flat configuration daily optical yield	EW flat configuration daily optical yield	eLLO-like flat configuration daily optical yield	*Relative difference between the total absorbed energy of the NS flat and EW configuration*	*Relative difference between the total absorbed energy of the eLLO-like flat and NS flat configuration*	*Relative difference between the total absorbed energy of the eLLO-like flat and EW flat configuration*
21/06/2021	50.5%	41.3%	46.2%	18.1%	-9.2%	10.5%
21/12/2021	18.1%	25.6%	24.2%	-41.0%	24.9%	-5.9%

In summer solstice, the maximum daily optical efficiency is achieved for NS flat configuration (50.5%) while in winter solstice it is reached for the EW configuration (41.3%). Thus, NS implementation is better for summer days than EW implementation with a relative difference between total absorbed energy of the NS and EW implementation of 18.1%, i.e. the absorbed energy of NS configuration is 18.1% higher than the absorbed energy of EW configuration. Vice-versa for winter days, the relative difference is equal to -41.0%.

The total absorbed energy achieved, in summer solstice, by eLLO-like flat implementation is 9.2% lower than the NS configuration and 10.5% higher than the EW configuration and in winter solstice the total absorbed energy achieved by eLLO-like flat configuration is 24.9% higher than the NS flat configuration and 5.9% lower than the EW flat configuration. The daily optical performance of eLLO-like flat configuration is between the daily optical performance of reference NS and EW flat configurations for winter and summer solstices.

As observed by Abbas et al. [19], the optical performance of NS implementation is highly dependent on the season and EW implementation allows high optical performance each day at noon, but with low optical yield during the morning and evening. Thus, the eLLO orientation induces less absorbed energy compared to the optimal summer and winter. However, this orientation allows obtaining optical performances close to the efficiency of the optimal implementation for the given season.

The behavior of an implementation with such an orientation seems to be closer to the behavior of an EW implementation, which is not surprising since the orientation offset studied regarding the NS axis is greater than 45°. To conclude, considering both solstices, eLLO-like flat configuration can achieve high optical performance close to the performance of a NS implementation in summer and EW implementation in winter.

3.2. Inclination impact on optical performance

In the following, a similar approach as the orientation study is followed to evaluate the influence of tilted modules on the optical performance. The eLLO-like tilted configuration corresponds to a solar line composed of 6 tilted modules, as the configuration presented in Figure 10. It has to be noted that the modules are oriented as the eLLO's solar field and are tilted both in the longitudinal and transversal plane, described respectively by the angles β and γ. As for the orientation study, the solar position is calculated in the module reference system and the transition matrix in this case requires simplifying hypotheses on the two successive rotations related to the longitudinal and transversal tilt. For the 6 modules, longitudinal tilt and transversal tilt are considered the same and are respectively 2.44° and 4.05°. The slopes correspond to the average slope of the 170 modules of the eLLO solar power plant. The total absorbed power and daily optical yield of eLLO-like tilted implementation are evaluated to be compared to the eLLO-like flat configuration, described in paragraph 3.1.

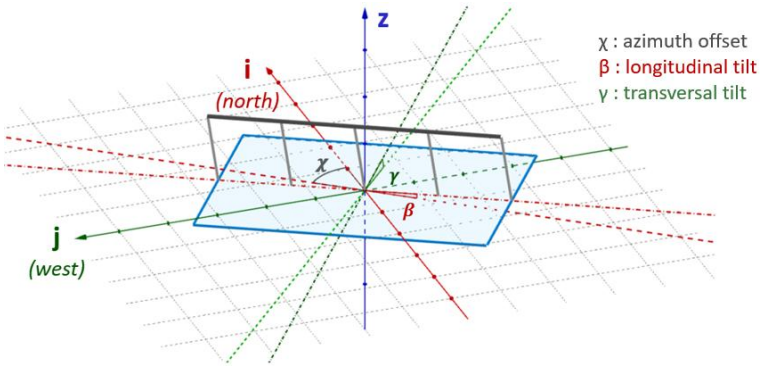

Figure 10 : Oriented and tilted configuration

The absorbed solar powers evolution during a day for both solstices are shown, in Figure 11, for the flat and eLLO-like tilted configuration.

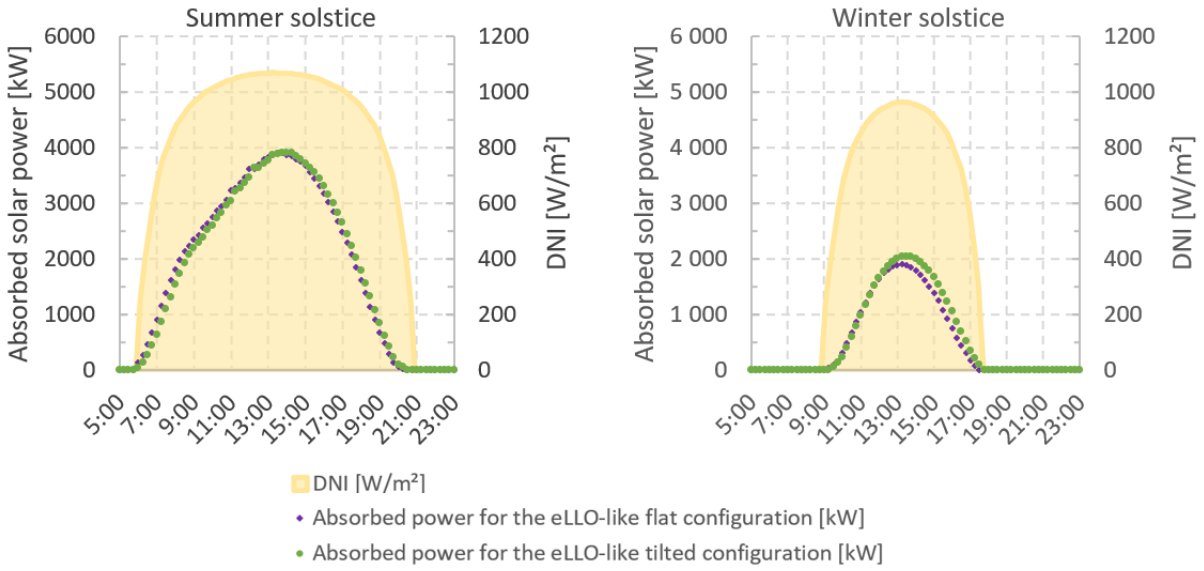

Figure 11 : Absorbed solar power by flat and eLLO-like tilted configuration for both solstices

For summer solstice day, Figure 11 shows that tilted configuration induced lower absorbed power in the morning and higher absorbed power after 3 PM than flat configuration. An identical behavior is observed for the winter solstice day with a more important difference between the two configurations.

The integrated daily results of the inclination impact study are summarized in Figure 12 and Table 7.

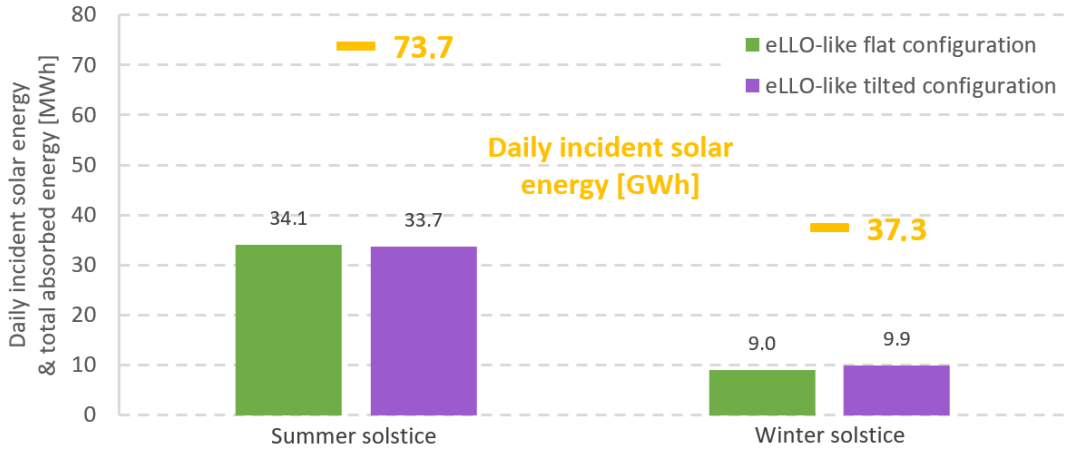

Figure 12 : Total absorbed energy for flat and titled configuration for both solstices

Table 7: Daily optical yield for flat and tilted configurations for both solstices' days

Day	eLLO-like flat configuration daily optical yield	eLLO-like tilted configuration daily optical yield	*Relative difference between the total absorbed energy of eLLO-like tilted and flat configuration*
21/06/2021	46.2%	45.7%	-1.1%
21/12/2021	24.2%	26.6%	10.3%

In summer solstice, the maximum daily optical efficiency is achieved for eLLO-like flat configuration (46.2%) while in winter solstice it is reached for the eLLO-like tilted configuration (26.6%). Thus, flat implementation is better for summer days than tilted implementation with a relative difference between total absorbed energy of -1.1% and vice-versa, for winter days, the relative difference is equal to 10.3%. Thus, the module array inclination allows greater solar energy capture in winter than a flat configuration and the summer optical performance is only slightly lower than flat configuration.

Note that in both solstices, the total absorbed energy in the morning is almost the same and, in the afternoon, the tilted configuration reaches higher total absorbed power than flat configuration.

Considering that solar energy resource is lower during winter, this may be an advantage of eLLO-like tilted configuration. To investigate more precisely this conclusion, the next subsection will focus on the annual behavior of such implementations.

3.3. Annual optical study for each configuration

Finally, an annual optical study of a NS and EW flat configurations and eLLO-like flat and tilted configuration is performed using the same method as the daily study with a 1 h resolution and clear sky DNI. The annual optical yield is evaluated in the same way as the daily yield by replacing, in equation (11) and (12), the daily time interval with an annual time interval. The results are summarized in Figure 13 and Table 8.

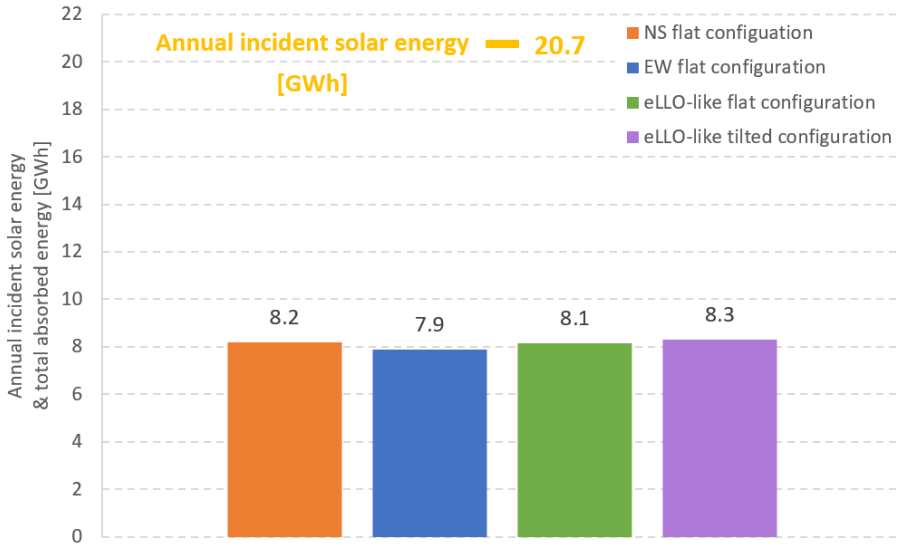

Figure 13 : Total absorbed energy for NS, EW flat configuration and eLLO-like flat and tilted configuration on an annual basis

Table 8: Annual optical yield for NS, EW flat configuration and eLLO-like flat and tilted configuration on an annual basis

NS flat configuration annual optical yield	**EW flat configuration annual optical yield**	**eLLO-like flat configuration annual optical yield**	**eLLO-like tilted configuration annual optical yield**	***Relative difference between the total absorbed energy of the NS and EW flat configuration***	***Relative difference between the total absorbed energy of the eLLO-like flat and NS flat configuration***	***Relative difference between the total absorbed energy of the eLLO-like tilted and NS flat configuration***
39.4%	37.9%	39.2%	39.9%	3.6%	-0.4%	1.4%

The annual optical yield for NS implementation is around 39.4%, while if the solar line is oriented EW the annual optical yield is 37.9%, i.e. a relative difference of 3.6% between the total absorbed energy. Thus, the NS flat implementation is slightly more effective than an EW flat implementation for localization of the eLLO project. In terms of annual solar-electricity efficiencies, Abbas et al. [20] show that NS and EW configuration solar fields located in Almería (37.1°N, -2.35°W), Spain achieve similar performance. Additionally, Sharma et al. [21] observed from their analysis of a collector of linear Fresnel reflector field located in Murcia (38.27°N, 1.6°W), Spain, a greater annual energy collection for NS configuration. Thus, the 40th parallels seem to be the limit beyond which EW configuration is more efficient over the year than NS implementation.

The eLLO-like flat configuration achieves, on an annual basis, almost the optical performance of a NS implementation, with a relative difference between the total absorbed energy of -0.4%. Moreover, the total absorbed energy of the eLLO-like tilted configuration is higher than the total absorbed energy of the NS implementation, with a relative difference of 1.4%. The maximum annual optical yield of

39.9% is obtained for the eLLO-like tilted configuration, which is slightly higher than the annual optical yield of the NS implementation.

Finally, the eLLO-like flat configuration with a tilt of approximately 2.5° in the transversal plane and 4° in the longitudinal plane leads to an increase in the optical performance by 1.8% compared to the eLLO-like flat configuration. Thus, the tilted configuration can achieve higher optical efficiency due to the module's inclination toward the south-west, which leads to solar positions in the module reference system close to the module zenith and therefore to the maximum optical performance of eLLO's module. Abbas et al. [18] observe a similar trend, by showing that the optical performance of EW oriented solar field is 4.4% lower than the optical performance of EW oriented solar field with a 7.5° tilt toward South.

Lastly, a similar optical study is performed for tilted configuration equipped with symmetrical modules (mirrors with focal lengths from 1 to 7 on each side of the module) to compare with the eLLO-like tilted configuration composed of asymmetrical modules. IAMs for symmetrical modules are determined using the same method as for an asymmetric module. The annual absorbed energy of the tilted configuration with symmetrical modules is equal to 8.21 MWh, which is lower than the annual absorbed energy of eLLO-like tilted configuration (8.28 MWh) and corresponds to a relative difference between these two arrays of 0.84%. Thus, in addition to the solution of compensating topographical constraints by adapting the module's configuration, the module design can be tailored to optimize the solar energy capture over the year.

After the analysis of the separated impacts of the orientation and inclination of the LFC modules, the next section will focus on the eLLO solar power plant case study.

4. Case study: the eLLO solar power plant

The specific topography of the implementation site of the eLLO power plant (Figure 1) induces individual configuration of each module and therefore different optical efficiencies for each module of a solar line. In this part, the modelled solar line is composed of 6 modules (M1 to M6) oriented as the eLLO's solar field and with individual inclination as described in the Table 9 to represent a solar line of the solar power plant. Based on the same methodology presented in the previous subsection, an optical study is performed to estimate the annual absorbed energy of the eLLO's solar line for a clear sky DNI but adding a solar mask to evaluate the solar incidence energy for the localization of the eLLO solar power plant, presented in appendix Figure A.2. As annual optical yield, the interval time is replaced in equation (11) and (12) by a monthly time interval.

Table 9: Longitudinal and transversal tilt of the 6 modules (M) of one eLLO's solar line

Transversal tilt γ [°] **Same for M1 to M6**	**Longitudinal tilt β [°]**					
	M1	*M2*	*M3*	*M4*	*M5*	*M6*
-4.01	-3.88	-2.90	-2.82	-2.56	-1.58	-1.19

Since the modules are individually inclined in the longitudinal plane, the connection between each module admits a break, that is not considered in the IAM definition. Thus, the optical losses due to the slope break between each module is neglected.

The simulation results, presented in

Figure 14, are expressed in monthly optical yield and compared to the conventional NS and EW flat implementations.

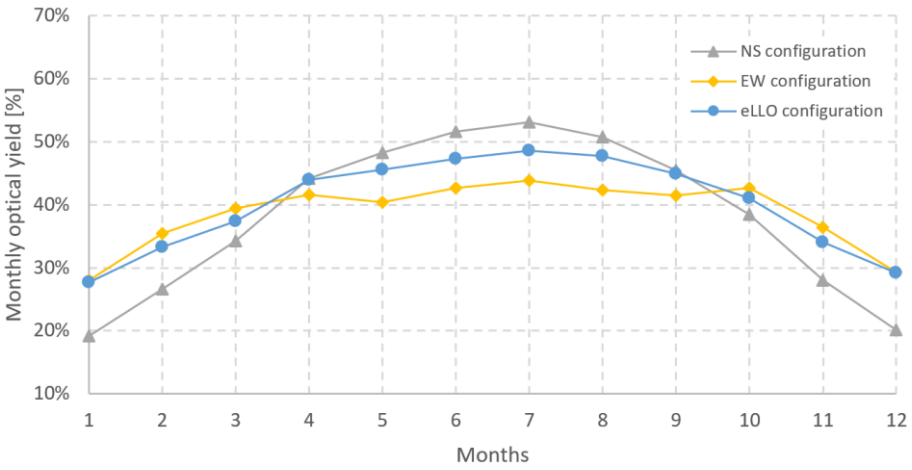

Figure 14 : Monthly optical yield for NS, EW and eLLO configuration

These results show the seasonality of a NS implementation and the attenuation of this effect with an EW implementation. From April to September, the NS implementation achieves better monthly optical yield than the EW implementation and the eLLO implementation. For the remaining months, it is the EW implementation that gives higher monthly optical yields than a NS flat configuration and slightly higher than the eLLO configuration. It should be noted that, for months around equinoxes, the yields of each configuration are close. To conclude on the optical efficiency of the eLLO's solar line and the influence of the topography on its optical performance, the annual absorbed power for these configurations, are integrated, and the results are presented in Figure 15 and Table 10.

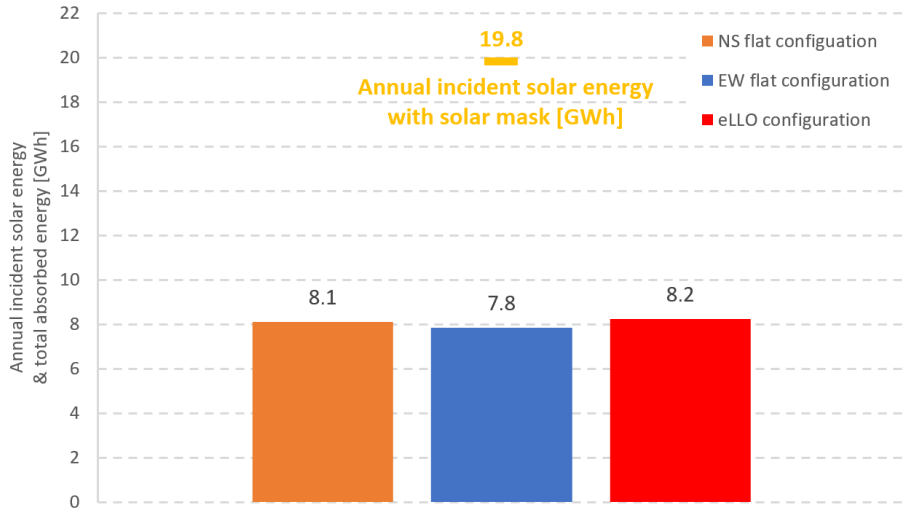

Figure 15 : Total absorbed energy for NS, EW flat configuration and eLLO configuration on an annual basis

Table 10: Annual optical performance for NS, EW and eLLO configuration on an annual basis

NS flat orientation annual optical yield [%]	EW flat orientation annual optical yield [%]	eLLO configuration annual optical yield [%]	Relative difference between the total absorbed energy of the eLLO and NS configuration	Relative difference between the total absorbed energy of the eLLO and EW configuration
41.0%	39.6%	41.6%	1.6%	4.9%

The annual optical yield of the eLLO's solar line is equivalent to 41.6% slightly higher than NS flat configuration efficiency equal to 41.0% and higher than EW flat configuration efficiency equal to 39.6%. The relative difference between total absorbed energy by the eLLO configuration and the NS and EW configurations are equal to 1.6% (eLLO-NS) and 4.9% (eLLO-EW) respectively.

Of course, the small relative difference between eLLO and NS configuration is not significant but shows that an LFC implementation project can be adapted to a specific topography by playing on the solar module configurations as well as on the module design. It should be noted that the topography of the eLLO's site is advantageous because the versant is facing southwest. Thus, despite the constraints of the topography, it was possible to define a specific configuration that was able to achieve better optical efficiency than NS and EW reference configurations for the eLLO solar power plant localization.

5. Conclusion

The influence of topography on the optical performance of a Fresnel solar field can be computed using MCRT models. This method allows studying any possible configuration of LFC modules. The optical study carried out in the present work has led to the following conclusions:

- For eLLO power plant localization, among the conventional NS or EW configurations, the NS orientation is the most efficient implementation despite the strong seasonal dependence of the optical performance of such a system.
- The orientation of eLLO solar power plant allows obtaining optical performances close to the efficiency of the optimal implementation for the given season, i.e. NS orientation for summer and EW orientation for winter. As for an EW configuration, it can help to even the production over the year and be a good strategy to ensure high optical performance during summer while limiting the seasonality issue of NS implementations.
- A tilted module array toward the southwest can allow greater solar energy capture than a flat implementation. Nevertheless, if considering a flat implementation site, this optimization of the solar field can lead to additional construction costs for mechanical structures, and become economically unacceptable. However, in the case of specific topography, solar field inclination could be imposed and can be used to the advantage of solar concentration.
- The use of asymmetrical distribution of primary reflectors bending radius allows optimizing the optical performance based on the solar position over the year.
- Despite the topographical constraints, SUNCNIM has defined a specific configuration and module design to achieve optical efficiency close to the efficiency of the conventional NS implementation. Thus, these optimizations make it possible to compensate the effect of the topography.

Acknowledgements

This work was supported by the program "Investissements d'Avenir" Labex Solstice managed by the National Research Agency [ANR-10-LABX-22-01] and by the National Agency for Technological Research [CIFRE contract n° 2020/0451, 2021].

References

[1] "IEA - International Energy Agency," 2022 [Online]. Available: https://www.iea.org/.

[2] Papadis, E., and Tsatsaronis, G., 2020, "Challenges in the Decarbonization of the Energy Sector," Energy, **205**, p. 118025.

[3] Baharoon, D. A., Rahman, H. A., Omar, W. Z. W., and Fadhl, S. O., 2015, "Historical Development of Concentrating Solar Power Technologies to Generate Clean Electricity Efficiently – A Review," Renew. Sustain. Energy Rev., **41**, pp. 996–1027.

[4] "National Renewable Energy Laboratory - NREL," 2021 [Online]. Available: https://www.nrel.gov/.

[5] Liu, M., Steven Tay, N. H., Bell, S., Belusko, M., Jacob, R., Will, G., Saman, W., and Bruno, F., 2016, "Review on Concentrating Solar Power Plants and New Developments in High Temperature Thermal Energy Storage Technologies," Renew. Sustain. Energy Rev., **53**, pp. 1411–1432.

[6] Zhu, G., Wendelin, T., Wagner, M. J., and Kutscher, C., 2014, "History, Current State, and Future of Linear Fresnel Concentrating Solar Collectors," Sol. Energy, **103**, pp. 639–652.

[7] Guo, S., Liu, D., Chu, Y., Chen, X., Xu, C., Liu, Q., and Guo, T., 2017, "Dynamic Behavior and Transfer Function of Collector Field in Once-through DSG Solar Trough Power Plants," Energy, **121**, pp. 513–523.

[8] Morin, G., Dersch, J., Platzer, W., Eck, M., and Häberle, A., 2012, "Comparison of Linear Fresnel and Parabolic Trough Collector Power Plants," Sol. Energy, **86**(1), pp. 1–12.

[9] Chaitanya Prasad, G. S., Reddy, K. S., and Sundararajan, T., 2017, "Optimization of Solar Linear Fresnel Reflector System with Secondary Concentrator for Uniform Flux Distribution over Absorber Tube," Sol. Energy, **150**, pp. 1–12.

[10] López-Alvarez, J. A., Larraneta, M., Silva-Pérez, M. A., and Lillo-Bravo, I., 2020, "Impact of the Variation of the Receiver Glass Envelope Transmittance as a Function of the Incidence Angle in the Performance of a Linear Fresnel Collector," Renew. Energy, **150**, pp. 607–615.

[11] He, J., Qiu, Z., Li, Q., and Zhang, Y., 2012, "Optical Design of Linear Fresnel Reflector Solar Concentrators," Energy Procedia, **14**(2011), pp. 1960–1966.

[12] Abbas, R., and Martínez-Val, J. M., 2015, "Analytic Optical Design of Linear Fresnel Collectors with Variable Widths and Shifts of Mirrors," Renew. Energy, **75**, pp. 81–92.

[13] Mathur, S. S., Kandpal, T. C., and Negi, B. S., 1991, "Optical Design and Concentration Characteristics of Linear Fresnel Reflector Solar Concentrators-II. Mirror Elements of Equal Width," Energy Convers. Manag., **31**(3), pp. 221–232.

[14] Babu, M., Sekhar Babu, P., Raj, S. S., and Saravanan, S., 2021, "Theoretical Design, Material Study and Material Selection for Compact Linear Fresnel Reflector Concentrating System," Mater. Today Proc., **45**(xxxx), pp. 1671–1678.

[15] Balaji, S., Reddy, K. S., and Sundararajan, T., 2016, "Optical Modelling and Performance Analysis of a Solar LFR Receiver System with Parabolic and Involute Secondary Reflectors,"

Appl. Energy, **179**, pp. 1138–1151.

[16] Barbón, A., Bayón-Cueli, C., Bayón, L., and Rodríguez, L., 2019, "Investigating the Influence of Longitudinal Tilt Angles on the Performance of Small Scale Linear Fresnel Reflectors for Urban Applications," Renew. Energy, **143**, pp. 1581–1593.

[17] Alrwashdeh, S. S., 2018, "Energy Production Evaluation from a Linear Fresnel Reflectors Arrays with Different Array Orientation," Int. J. Eng. Res. Technol., **11**(11), pp. 1811–1819.

[18] Abbas, R., Valdés, M., Montes, M. J., and Martínez-Val, J. M., 2017, "Design of an Innovative Linear Fresnel Collector by Means of Optical Performance Optimization: A Comparison with Parabolic Trough Collectors for Different Latitudes," Sol. Energy, **153**, pp. 459–470.

[19] Abbas, R., Montes, M. J., Rovira, A., and Martínez-Val, J. M., 2016, "Parabolic Trough Collector or Linear Fresnel Collector? A Comparison of Optical Features Including Thermal Quality Based on Commercial Solutions," Sol. Energy, **124**, pp. 198–215.

[20] Sebastián, A., Abbas, R., Valdés, M., and Casanova, J., 2018, "Innovative Thermal Storage Strategies for Fresnel-Based Concentrating Solar Plants with East-West Orientation," Appl. Energy, **230**(August), pp. 983–995.

[21] Sharma, V., Nayak, J. K., and Kedare, S. B., 2015, "Effects of Shading and Blocking in Linear Fresnel Reflector Field," Sol. Energy, **113**, pp. 114–138.

[22] Bittencourt de Sá, A., Pigozzo Filho, V. C., Tadrist, L., and Passos, J. C., 2021, "Experimental Study of a Linear Fresnel Concentrator: A New Procedure for Optical and Heat Losses Characterization," Energy, **232**.

[23] Montes, M. J., Rubbia, C., Abbas, R., and Martínez-Val, J. M., 2014, "A Comparative Analysis of Configurations of Linear Fresnel Collectors for Concentrating Solar Power," Energy, **73**, pp. 192–203.

[24] Danish, S. N., Al-Ansary, H., El-Leathy, A., Ba-Abbad, M., Khan, S. U.-D., Rizvi, A., and Jamel, O., 2022, "Experimental and Techno-Economic Analysis of Two Innovative Solar Thermal Receiver Designs for a Point Focus Solar Fresnel Collector," Energy, **261**(PA), p. 125035.

[25] "SolarPACES," 2021 [Online]. Available: https://www.solarpaces.org/csp-technologies/csp-projects-around-the-world/.

[26] Beltagy, H., 2021, "The Effect of Glass on the Receiver and the Use of Two Absorber Tubes on Optical Performance of Linear Fresnel Solar Concentrators," Energy, **224**, p. 120111.

[27] Hack, M., Zhu, G., and Wendelin, T., 2017, "Evaluation and Comparison of an Adaptive Method Technique for Improved Performance of Linear Fresnel Secondary Designs," Appl. Energy, **208**(September), pp. 1441–1451.

[28] Ko, G. K., 2019, "Etude et Modélisation Dynamique d ' Un Concentrateur à Miroir Linéaire de Fresnel Gaelle Kafira Ko To Cite This Version : HAL Id : Tel-02368068."

[29] Rabl, A., 1976, "Comparison of Solar Concentrators," Sol. Energy, **18**(2), pp. 93–111.

[30] Sarver, T., Al-Qaraghuli, A., and Kazmerski, L. L., 2013, "A Comprehensive Review of the Impact of Dust on the Use of Solar Energy: History, Investigations, Results, Literature, and Mitigation Approaches," Renew. Sustain. Energy Rev., **22**, pp. 698–733.

[31] Garcia, P., Ferriere, A., and Bezian, J. J., 2008, "Codes for Solar Flux Calculation Dedicated to Central Receiver System Applications: A Comparative Review," Sol. Energy, **82**(3), pp. 189–197.

[32] Blanco, M., Mutuberria, A., Monreal, A., and Albert, R., 2011, "Results of the Empirical Validation of Tonatiuh at Mini-Pegase CNRS-PROMES Facility.," Proc SolarPACES.

[33] Blanco, M. J., Mutuberria, A., and Martinez, D., 2010, "Experimental Validation of Tonatiuh Using the Plataforma Solar de Almería Secondary Concentrator Test Campaign Data.," *In 16th Annual SolarPACES Symposium.*

[34] Buie, D., Monger, A. G., and Dey, C. J., 2003, "Sunshape Distributions for Terrestrial Solar Simulations," Sol. Energy, **74**(2), pp. 113–122.

[35] Schubnell, M., 1992, "Sunshape and Its Influence on the Flux Distribution in Imaging Solar Concentrators," **114**(November 1992).

[36] Zhu, G., 2013, "Development of an Analytical Optical Method for Linear Fresnel Collectors," Sol. Energy, **94**, pp. 240–252.

[37] Mertins, M., 2009, "Technische Und Wirtschaftliche Analyse von Horizontalen Fresnel-Kollektoren," p. 127.

[38] Eck, M., Hirsch, T., Feldhoff, J. F., Kretschmann, D., Dersch, J., Gavilan Morales, A., Gonzalez-Martinez, L., Bachelier, C., Platzer, W., Riffelmann, K. J., and Wagner, M., 2014, "Guidelines for CSP Yield Analysis - Optical Losses of Line Focusing Systems; Definitions, Sensitivity Analysis and Modeling Approaches," Energy Procedia, **49**, pp. 1318–1327.

[39] Rodat, S., Bavière, R., Bruch, A., and Camus, A., 2018, "Dynamic Simulation of a Fresnel Solar Power Plant Prototype with Thermocline Thermal Energy Storage," Appl. Therm. Eng., **135**(August 2017), pp. 483–492.

[40] Novatec solar, "Technical Data NOVA-1."

[41] Solar, I., 2009, "Technical Data Industrial Solar LF-11."

[42] Grena, R., 2012, "Five New Algorithms for the Computation of Sun Position from 2010 to 2110," Sol. Energy, **86**(5), pp. 1323–1337.

[43] Bird, R. E., and Hulstrom, R. L., 1981, "A Simplified Clear Sky Model for Direct and Diffuse Insolation on Horizontal Surfaces," Sol. Energy Res. Inst.

Appendix A

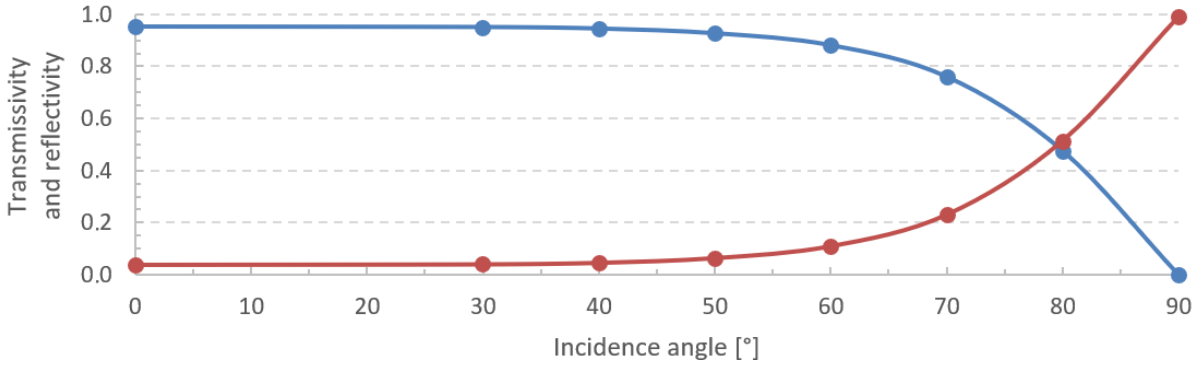

Figure A.1: Angle-dependent optical properties of the glass cover

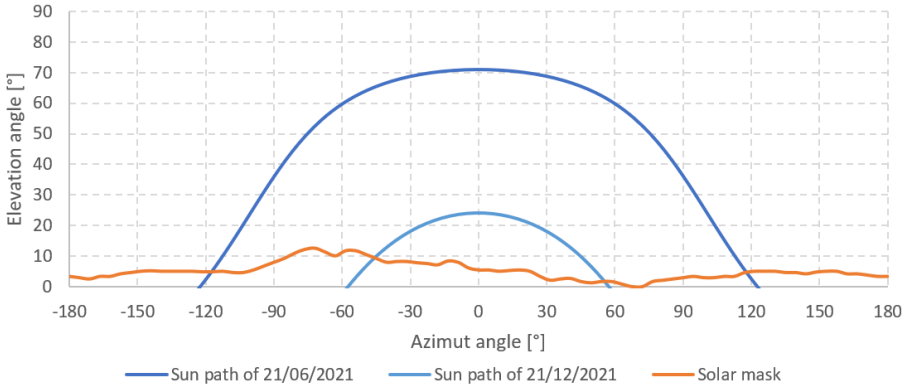

Figure A.2: The eLLO's solar mask and the solar path on 21/06/2021 and 21/12/2021